On the Formation and Breakup of Spiral Waves of Calcium

A. McKenzie*and J. Sneyd†

October 21, 1998

Abstract

We study spiral waves in a model of Ca^{2+} dynamics in the *Xenopus laevis* oocyte. Spiral waves in the model were initiated by simulating the release of inositol 1,4,5-trisphosphate (IP_3), a common experimental protocol. No artificial heterogeneities need to be imposed on the system for the spontaneous formation of spiral waves. Increasing the size of the IP_3 additions caused a decrease in the rotation period, and the breakup of the spiral wave solutions. After the breakup of a spiral wave, irregular spatio-temporal patterns occurred. Similar disorganised patterns are sometimes seen experimentally; based on our simulations we predict that a simple experimental procedure may be sufficient to reproduce unstable spiral waves.

*Department of Mathematics, University of Canterbury, Christchurch, New Zealand

†Department of Mathematics, University of Michigan, East Hall, 525 East University Avenue, Ann Arbor, MI 48109-1109, U.S.A. jsneyd@math.lsa.umich.edu. To whom correspondence should be addressed

1 Introduction

In practically every cell type, Ca^{2+} plays a major role in the control of cellular behaviour, functioning as a signalling agent for a variety of cellular processes such as chemical secretion, cell division, and cell movement. Oscillations in the concentration of free intracellular Ca^{2+} have been observed in very many cell types, and it is widely believed that the frequency of these oscillations is one way in which Ca^{2+} may carry an intracellular signal. High concentrations of Ca^{2+} inside cells are toxic, and thus a Ca^{2+} oscillation lets the cell use Ca^{2+} as an intracellular messenger, while avoiding prolonged high Ca^{2+} concentrations which would kill the cell. There has thus been a great deal of recent interest in the mechanisms underlying oscillatory Ca^{2+} responses to various extracellular signals, such as hormones or neurotransmitters. Experimental work has uncovered many of the basic mechanisms that lead to Ca^{2+} oscillations, but the mechanisms involved are complex and the details are unclear.

Study of Ca^{2+} oscillations is complicated by the fact that, in most cell types, the oscillations do not occur in a spatially homogeneous fashion, but instead take the form of periodic intracellular waves. When a cell is large enough, these periodic waves can exhibit more complex spatio-temporal organisation. For instance, in the *Xenopus laevis* oocyte (a very large cell with a diameter of up to 1000 μm) a variety of wave behaviour has been observed including plane waves, pulsating patterns, and spiral waves. *Xenopus* oocytes are thus an ideal cell type for the study of the mechanisms underlying Ca^{2+} wave propagation, and have been studied correspondingly intensely [Lechleiter & Clapham 1992, Lechleiter, Girard, Peralta & Clapham 1991, Lechleiter, Girard, Clapham & Peralta 1991].

There are a number of models for Ca^{2+} wave propagation [Goldbeter et al. 1990, Somogyi & Stucki 1991, DeYoung & Keizer 1992, Li & Rinzel 1994, Sneyd et al. 1995], all of which show a great deal of fundamental similarity. Here we shall use only the model developed by Atri et al. [1993], a model that was developed using, wherever possible, parameter values determined from *Xenopus*.

2 The biological mechanism

There is widespread agreement on the initial steps of the process that leads eventually to Ca^{2+} waves. When a hormone or neurotransmitter binds to its receptor it initiates a series of reactions that ends in the formation of a chemical called inositol 1,4,5-

trisphosphate (IP_3) (Fig. 1). IP_3 diffuses through the cell cytosol where it binds to receptors located on the endoplasmic reticulum (ER), and probably the nucleus also. The IP_3 receptors are also Ca^{2+} channels, and when they bind IP_3 they open, which lets Ca^{2+} flow out of the ER. In this context it is important to note that, at rest, the ER expends a great deal of energy pumping Ca^{2+} out of the cytoplasm into the ER. Thus there is a very large Ca^{2+} concentration gradient across the ER membrane. As Ca^{2+} is present at very high concentration outside the cell also, there is also a large Ca^{2+} gradient across the external membrane. However, this plays a minor role in *Xenopus* (although not in all cell types).

The open probability of the IP_3 receptor is modulated by both IP_3 and Ca^{2+}, a system of controls that is believed to underlie Ca^{2+} oscillations and waves in many cell types, including *Xenopus*. An increase in the cytosolic Ca^{2+} concentration causes a transient increase in the open probability of the IP_3 receptor, as Ca^{2+} first activates the receptor and then, on a slower time scale, inactivates it. Furthermore, the steady state open probability of the receptor is a bell-shaped function of Ca^{2+}. Thus, the dual action of Ca^{2+} on the receptor can be seen both in the transient and the steady state responses.

IP_3 and Ca^{2+} diffuse through the cytosol inducing further release of Ca^{2+}, and the Ca^{2+} released from the ER is pumped back into the ER or out of the cell. IP_3 is metabolised into a variety of other inositol phosphates whose function in many cases is unknown [Putney & Bird 1993]. In essence, the cytoplasm of the cell can form an excitable medium. The release of a small amount of Ca^{2+} through the IP_3 receptor causes the release of a much greater amount, in a positive feedback process called calcium-induced calcium release, or CICR. It is this excitability, linked by Ca^{2+} diffusion, that is believed to underlie the propagation of Ca^{2+} waves in many circumstances. However, when the concentration of IP_3 is in some intermediate region (which we show explicitly later) a stable limit cycle appears in the kinetics, and thus the model becomes oscillatory. For these IP_3 concentrations, wave propagation can occur even in the absence of excitability. Because of the technical difficulties involved in the measurement of IP_3 concentrations, it is not yet clear whether spiral waves in *Xenopus* cytoplasm occur in the excitable regime, or in the self-oscillatory regime.

In *Xenopus* oocytes, Ca^{2+} waves travel at speeds ranging from 10–30 μms^{-1}; the spiral waves have period around 6–10 seconds, and wavelength around 200 μm [Lechleiter & Clapham 1992, Lechleiter, Girard, Peralta & Clapham 1991]. Very little

work has been done on the dispersion properties of *Xenopus* cytoplasm, and the exact shape of the dispersion curve is not known.

3 Mathematical model

A partial differential equation model based on the mechanisms outlined above was developed by Atri et al. [1993]. The model assumes that the *Xenopus* cytoplasm is spatially homogeneous and continuous. Although these assumptions are known to be inaccurate in some parameter regions (for instance, at low IP_3 concentrations, Ca^{2+} release occurs at discrete hot spots [Lechleiter & Clapham 1992], which violates the assumption of homogeneity), for the kind of behaviour we shall study here they are sufficiently accurate, as we shall consider only the responses to large additions of IP_3.

Furthermore the partial differential equation model is in two dimensions instead of three dimensions. The principal reason for this is that some experimental data indicate that in the *Xenopus* oocyte the calcium wave activity is localised to a region near the surface of about 100μm thick [Parys et al. 1992]. More recent data, that show that wave activity can extend as far as 200 μm into the cell or even further, throw some doubt on whether or not this assumption is entirely defensible but that is not an issue we explore here. Therefore, as an approximation, the calcium wave activity may be modelled as a two-dimensional phenomenon.

Furthermore, we shall assume that the spirals live on a planar two-dimensional surface. Although the outer layer of the *Xenopus* oocyte is clearly spherical in geometry, the large diameter of the oocyte (about 1000 μm) compared to the wavelength of a typical spiral (150–200 μm) means that an assumption of planar geometry will be sufficiently accurate for our purposes.

We assume that IP_3 diffuses passively through the cytoplasm, and is not degraded. Thus

$$\frac{\partial P}{\partial t} = D_p(P_{xx} + P_{yy}), \tag{1}$$

where P denotes the concentration of IP_3. Thus, we are simulating experiments using non-hydrolysable analogues of IP_3 that are degraded only very slowly if at all.

Similarly, we assume that Ca^{2+} diffuses passively, is released through the IP_3 receptor (J_{channel}), is pumped into the internal store (J_{pump}), and leaks into the cell from the ER or from outside (J_{leak}). Thus, letting c denote the concentration of Ca^{2+}, we have

$$\frac{\partial c}{\partial t} = D_c(c_{xx} + c_{yy}) + J_{\text{channel}} - J_{\text{pump}} + J_{\text{leak}} \tag{2}$$

where

$$J_{\text{channel}} = k_{\text{flux}}\mu(P)h\left(b + \frac{(1-b)c}{k_1 + c}\right), \quad (3)$$

$$J_{\text{pump}} = \frac{\gamma c}{k_\gamma + c}, \quad (4)$$

$$J_{\text{leak}} = \beta, \quad (5)$$

$$\mu(P) = \mu_0 + \frac{\mu_1 P}{k_\mu + P}. \quad (6)$$

The expressions for J_{pump} and J_{leak} are straightforward, but J_{channel} is more complicated, being a product of three terms (k_{flux} is merely a scaling parameter); μ denotes the fraction of receptors that have bound IP_3, $b+(1-b)c/(k_1+c)$ denotes the fraction of receptors that have been activated by Ca^{2+}, while h denotes the fraction of receptors that have not been inactivated by Ca^{2+}. Activation by Ca^{2+} is assumed to act instantaneously, but inactivation by Ca^{2+} occurs on a slower time scale, and thus

$$\tau_h \frac{dh}{dt} = h_\infty(c) - h, \quad (7)$$

where

$$h_\infty(c) = \frac{k_2^2}{k_2^2 + c^2}. \quad (8)$$

This assumption of fast activation and slow inactivation is based on the experimental results of a number of groups [Finch et al. 1991, Parker & Ivorra 1990, Parker & Yao 1992].

The parameters for J_{channel} were chosen so as to agree with the experimental data of [Parys et al. 1992]. It is important to note that the pumping efflux measured by Parys et al. [1992] was at a steady state Ca^{2+} concentration. When the Ca^{2+} concentration is changing, as it does during oscillations, the rate at which the channel activates and inactivates is important in determining the Ca^{2+} concentration flux.

J_{pump} models the pumping of Ca^{2+} out of the cytosol and is a simple hyperbolic function of c. The term J_{leak} represents a flux due to leakage into the cytosol from outside the cell. In many experiments with *Xenopus* in which Ca^{2+} waves were observed, the extracellular Ca^{2+} concentration was maintained at very low levels [Lechleiter & Clapham 1992]. Because of this leakage through the cell membrane was very small. Therefore the term J_{leak} was set to zero for all the simulations. A non-zero leak makes no qualitative difference to our results.

The parameter values used in the model are shown in Table 1. Parameter values were chosen to match up with known experimental results, where these were available. Note that the diffusion coefficient of Ca^{2+} is set at a low value to simulate the effects of Ca^{2+} buffering [Sneyd et al. 1995].

An insight into the type of solutions the model has may be gained by considering the spatially homogeneous equations, that is, the equations without diffusion. At a constant IP_3 concentration

these equations are ordinary differential equations for which μ functions as a bifurcation parameter. The bifurcation diagram is given in Figure 2. A branch of periodic solutions appears via a Hopf bifurcation at $\mu = 0.5$, and disappears at a homoclinic bifurcation at about $\mu = 0.29$. When studied on a finer scale (Figure 2B) it can be seen that a lower Hopf bifurcation point also exists (at $\mu = 0.2926$) but the branch of periodic orbits arising from this bifurcation soon disappears in a homoclinic bifurcation when it intersects the branch of unstable steady states, and is thus of no physiological interest.

3.1 Numerical methods and initial conditions

The equation for P ($[IP_3]$) is a diffusion equation and was solved using the Peaceman-Rachford algorithm, an alternating-direction implicit method. The equation for c ($[Ca^{2+}]$) is a reaction-diffusion equation and was solved using a generalisation of the Peaceman-Rachford algorithm. With no flux boundary conditions, the resulting system of equations is tridiagonal, and was solved using the NAG fortran subroutine *f04lef*. The ordinary differential equation for h (the inactivation variable) was solved using a second order Taylor series approximation.

Unless otherwise stated, all simulations were run on a 200 by 200 square grid, and a time step of 0.05 seconds was used. After each time step the $[Ca^{2+}]$ values were output as a Hierarchal Data Format (HDF) file, and the collection of files were viewed using the scientific visualisation software *Transform* (Fortner Research). Dispersion curves, and branches of periodic orbits, were calculated using *AUTO* (written by E. Doedel et al., available from ftp.cs.concordia.ca), and *xppaut* (written by B. Ermentrout, available from ftp.math.pitt.edu).

We used a variety of initial conditions, all of the same basic form (Figure 3). At time $t = 0$ the $[IP_3]$ is set to a constant concentration (usually zero) over the grid. The $[Ca^{2+}]$ and h are set at the steady state values for that steady $[IP_3]$. The steady state is disrupted by adding boli of IP_3 at arbitrarily selected places in the domain (labelled blocks A, B, and C in the figure). There were no other imposed heterogeneities in the domain. For all simulations presented here we added IP_3 at the same places, in order to facilitate comparison between the simulations.

When the IP_3 boli are added IP_3 rapidly diffuses through the square. Within a short time ($\approx 50 - 100$ s) the $[IP_3]$ is nearly constant throughout the square, the concentration approaching a long term $[IP_3]$. Corresponding to the long term $[IP_3]$

is a bifurcation parameter μ value set by Eq. (6). The long term μ value and the long term [IP_3] were recorded for each simulation.

4 Results

4.1 Initiation of stable spiral waves

Numerically computed spiral waves in this model, quantitatively similar to those seen experimentally, have been found by Atri *et al.* (1993). Atri *et al.* (1993) first initiated periodic plane waves by the release of a bolus of IP_3, and then used arbitrarily selected regions to block passage of the waves, leading to breakage of the wave front, and consequent spiral formation. After a short time, the blocking regions were removed, and the spirals thus continued to rotate in a homogeneous medium. However, one major criticism of these computations has been that spirals were initiated by artificial conditions that were not likely to exist in the cell, as it was difficult to justify the assumption of temporary blocking regions on purely physiological grounds.

In Figure 4 we show how spirals may be initiated in the Atri model without the use of any artificially imposed blocking regions. Three boli of IP_3 are released in the cell at arbitrarily selected positions, as shown in Figure 3. The released IP_3 is then allowed to diffuse across the cell, releasing Ca^{2+} as it does so. The diffusion of IP_3 sets up a natural heterogeneity in the cell cytoplasm such that multiple spirals begin to form spontaneously by 300 seconds. Note that, apart from the heterogeneity resulting from the diffusion of IP_3, the cell cytoplasm is homogeneous in all other respects; there are no artificial blocking regions. By 1600 seconds the spirals have taken over the entire domain, and comparison of the panels for 1600 and 2000 seconds shows that the spiral centers are rotating slowly around each other. Thus, the spirals are not stationary. This behavior persists up to at least 4000 seconds (computations not shown). At long times, the concentration of IP_3 is approximately constant at 2.012 μM, which corresponds to $\mu = 0.3904$. From Fig. 2 we note that this value is well within the region where the kinetics are self-oscillatory.

4.2 Breakup of spiral waves, and periodically spiral waves

Calcium waves in *Xenopus* can sometimes form spatio-temporal patterns considerably more complex than simple spirals. In an effort to gain some understanding of this more complex wave behaviour, we wish to investigate under what conditions the spiral wave solutions persist, or whether breakup of the

spirals can lead to more complex behaviour. In order for the results to be useful, we wish further to show that spiral breakup can be generated by a procedure that can be reproduced in the laboratory.

In Figure 5, we show the result of a computation similar to that shown in Figure 4, except that now the size of the bolus in block C is slightly increased. In this simulation, the long term value of μ is 0.39547, which corresponds to a steady IP_3 concentration of about 2.17 μM. By 900 seconds, the central spiral has formed, but the smaller spirals around its edge have broken up to disordered behavior. Interestingly, at 1200 seconds we see that the central spiral itself starts to breakup, but by 1500 seconds has spontaneously reformed. This periodic appearance and disappearance of the spirals is a characteristic feature of our simulations; we call these kinds of waves *periodically spiral* waves.

When the size of the IP_3 bolus in block C is increased still further (long term value of μ is 0.3965, $[IP_3]$=2.20 μM), we get an earlier, and more complete, breakup of the central spiral.

4.3 Discussion

We have shown that spiral waves can be initiated by a procedure that mimics experimental procedures. Simple addition of IP_3 in a number of different places can lead spontaneously to spiral wave formation. No artificial heterogeneities need to be imposed on the system, apart from those arising naturally as the result of the heterogeneous distribution of IP_3.

By varying the size of the IP_3 additions, we can generate different long-term IP_3 concentrations; as the long-term $[IP_3]$ increases, the spirals become unstable, and break up to form irregular spatio-temporal patterns. This instability is not caused by the slight heterogeneities that exist in $[IP_3]$ at large times. We showed this by simulations in which the background IP_3 was set to be constant (at its steady state value) once the spiral had formed, but before it had broken up (for instance, at time 500 seconds in Figure 5). In these simulations (not shown here) the spirals still broke up in the same manner. In our simulations, spiral breakup occured first at the spiral core, when the wave given off by the core intersected the refractory region behind the previous wave; this mechanism for destabilising spirals has been described before in other models [Panfilov & Holden 1991].

As shown in Figure 7, the spiral period decreases with increasing long term IP_3 concentration. If the spiral period is less than a critical value of about 8.5 seconds then the spiral is unstable. Other models, such as the Noble model for cardiac tis-

sue, also have a critical value for the rotation period [Karma 1993]. However, the exact reasons for this critical spiral period in this model are unclear. Close to the critical spiral period, the spiral core breaks up and reforms in a regular manner, leading to the formation of what we call periodically spiral waves. In these simulations the spirals that form can take over considerable portions of the domain before finally going unstable and breaking up, whereupon the core reforms and begins to form another spiral which can itself grow to considerable size before it breaks up. Further away from the critical period, spirals do not reform to any significant extent.

The domain size is important in determining the long term behaviour of the system. With the same long term IP_3 concentration, but with a smaller domain of 250 μm by 250 μm, the spiral waves become unstable at lower steady state IP_3 concentrations (computations not shown). Thus on a smaller domain the patterns that form are less stable, a result that has been proven for spiral waves in an oscillatory medium [Paullet et al. 1994].

Our results predict that a dose-response series of IP_3 additions will lead to destabilisation of the observed spiral waves, and irregular behaviour. Such dose-response experiments have been performed in *Xenopus* by Parker and his colleagues [Parker & Yao 1992] but have used low concentrations of IP_3, close to the threshold of wave propagation. To our knowledge, these experiments have not been performed at the higher IP_3 concentrations needed to test our predictions.

References

Atri, A., Amundson, J., Clapham, D. & Sneyd, J. [1993]. A single-pool model for intracellular calcium oscillations and waves in the Xenopus laevis oocyte, *Biophysical J.* **65**: 1727–1739.

DeYoung, G. & Keizer, J. [1992]. A single pool IP_3-receptor based model for agonist stimulated Ca^{2+} oscillations, *Proc. Natl. Acad. Sci. USA* **89**: 9895–9899.

Finch, E., Turner, T. & Goldin, S. [1991]. Calcium as a coagonist of inositol 1,4,5-trisphosphate-induced calcium release, *Science (Washington DC)* **252**: 442–446.

Goldbeter, A., Dupont, G. & Berridge, M. [1990]. Minimal model for signal-induced calcium oscillations and for their frequency encoding through protein phosphorylation, *Proc. Natl. Acad. Sci. USA* **87**: 1461–1465.

Karma, A. [1993]. Spiral breakup in model equations of action potential propagation in cardiac tissue, *Physical Review Letters* **71**(7): 1103–1106.

Lechleiter, J. & Clapham, D. [1992]. Molecular mechanisms of intracellular calcium excitability in X. laevis oocytes, *Cell* **69**: 283–294.

Lechleiter, J., Girard, S., Clapham, D. & Peralta, E. [1991]. Subcellular patterns of calcium release determined by G protein-specific residues of muscarinic receptors, *Nature* **350**: 505–508.

Lechleiter, J., Girard, S., Peralta, E. & Clapham, D. [1991]. Spiral calcium wave propagation and annihilation in Xenopus laevis oocytes, *Science* **252**: 123–126.

Li, Y. & Rinzel, J. [1994]. Equations for $InsP_3$ receptor-mediated $[Ca^{2+}]$ oscillations derived from a detailed kinetic model: a Hodgkin-Huxley like formalism, *J. Theor. Biol.* **166**: 461–473.

Panfilov A.V. & Holden A.V. [1991]. Spatiotemporal irregularity in a two-dimensional model of cardiac tissue, *Int. J. Bif. Chaos* **1**: 219–225.

Parker, I. & Ivorra, I. [1990]. Inhibition by Ca^{2+} of inositol trisphosphate mediated Ca^{2+} liberation: a possible mechanism for oscillatory release of Ca^{2+}, *Proc. Natl. Acad. Sci. USA* **87**: 260–264.

Parker, I. & Yao, Y. [1992]. Regenerative release of calcium from functionally discrete subcellular stores by inositol trisphosphate, *Proc. R. Soc. London B* **246**: 269–274.

Parys, J., Sernett, S., DeLisle, S., Snyder, P., Walsh, M. & Campbell, K. [1992]. Isolation, characterization, and localization of the inositol 1,4,5-trisphosphate receptor protein in Xenopus laevis oocytes, *J. Biol. Chem.* **267**: 18776–18782.

Paullet, J., Ermentrout, B. & Troy, W. [1994]. The existence of spiral waves in an oscillatory reaction-diffusion system, *SIAM J. Appl. Math* **54**(5): 1386–1401.

Putney, J. & Bird, G. [1993]. The inositol phosphate-calcium signaling system in nonexcitable cells, *Endocrine Reviews* **14**(5): 610–631.

Sneyd, J., Keizer, J. & Sanderson, M. [1995]. Mechanisms of calcium oscillations and waves: a quantitative analysis, *FASEB J.* **9**: 1463–1472.

Somogyi, R. & Stucki, J. [1991]. Hormone-induced calcium oscillations in liver cells can be explained by a simple one-pool model, *J. Biol. Chem.* **266**: 11068–11077.

Table Caption

Table 1: Parameter values for the model. Parameter values were chosen to match up with known experimental results, where these were available.

Figure Captions

Fig. 1: The biological mechanism for Ca^{2+} oscillations. A hormone or neurotransmitter binds to a receptor. This stimulates the activation of the enzyme phosphodiesterase (PLC), which catalyses the break up of phosphotidylinositol-(4,5)-bisphosphate (PIP_2) into inositol trisphosphate (IP_3) and diacylglycerol (DAG). Both IP_3 and DAG simulate further cellular responses, but via different reaction pathways. IP_3 diffuses through the cell cytosol where it activates receptors located on the endoplasmic reticulum (ER). This brings about the release of Ca^{2+} from the ER. The release of Ca^{2+} from the ER activates the further release of Ca^{2+} until, at higher Ca^{2+}, the receptor inactivates. Both IP_3 and Ca^{2+} diffuse through out the cytosol inducing further release of Ca^{2+}.

Fig. 2: A: Bifurcation diagram for the spatially homogeneous model equations, using μ (which is equivalent to $[IP_3]$) as the bifurcation parameter. HC, homoclinic bifurcation; HB, Hopf bifurcation; c_{ss}, steady state value of c; $c_{\max}$ and $c_{\min}$, maximum and minumum values of c over one oscillation. Dashed lines denote instability. A subcritical Hopf bifurcation occurs at $\mu = 0.5012$ and this generates a branch of periodic orbits, which is initially unstable but becomes stable in a saddle-node of periodics bifurcation. The branch of stable periodic orbits ends in a homoclinic bifurcation at $\mu \approx 0.29$. For μ slightly less than 0.2926 the system exhibits excitable behaviour. The parameter values for the model equations are shown in Table 1. B: a detailed view of the Hopf bifurcation at $\mu = 0.2926$. Around this value of μ a second branch of unstable periodic orbits appears, and then disappears in a second homoclinic bifurcation when it intersects the branch of unstable steady states.

Fig. 3: Initial conditions. At time $t = 0$ $[IP_3]$ is set to a constant value (usually zero), and $[Ca^{2+}]$ and h are set to the corresponding steady states. At time $t = 0$, boli of $[IP_3]$ are released in the indicated regions. The square size is $1000\mu m$ by $1000\mu m$, and the spatial grid is 200×200. The boundary conditions are no flux.

Fig. 4: Formation of stable spiral waves. Block A: $[IP_3]$=200 μM. Block B: $[IP_3]$=240 μM. Block C: $[IP_3]$=65 μM. Long term value of μ is 0.3904. Long term $[IP_3]$ is 2.012 μM.

Fig. 5: Formation of unstable spiral waves, and periodically spiral waves. Block A: $[IP_3]$=200 μM. Block B: $[IP_3]$=240 μM. Block C: $[IP_3]$=79 μM. At 1 second and 100 seconds, the simulations looks very similar to the results shown in Figure 4. Long term value of μ is 0.39547. Long term $[IP_3]$ is 2.17 μM. This value of μ is close to the boundary between instability and stability, and so large, regular spiral waves persist in large regions of the domain. Elsewhere, the spirals are much smaller, and do not persist, leading to more disordered behavior.

Fig. 6: Formation of unstable spiral waves, and periodically spiral waves. Block A: $[IP_3]$=200 μM. Block B: $[IP_3]$=240 μM. Block C: $[IP_3]$=82 μM. At 1 second and 100 seconds, the simulations looks very similar to the results shown in Figure 4. Long term value of μ is 0.3965. Long term $[IP_3]$ is 2.20 μM. The center spiral becomes unstable by 700 seconds, and reforms periodically, but never persists long enough to take over a significant portion of the domain. By 1200 seconds, irregular spatio-temporal behavior is seen over the entire domain.

Fig. 7: Spiral period and wave speed as a function of the steady state value of μ. As μ increases (i.e., as the background IP_3 increases), the spiral period decreases, due almost entirely to an increase in the wave speed, while the wavelength remains almost constant. However, once the spiral period is too low, the spiral cannot sustain itself; the wave given off by the spiral core runs into the refractory region behind the previous wave, which causes breakup of the spiral.

Table 1: Mckenzie and Sneyd

Parameter	Value
b	0.111
β	0.0
γ	2.0 $\mu\mathrm{M} \cdot \mathrm{s}^{-1}$
τ_h	2.0 s
k_1	0.7 μM
k_2	0.7 μM
k_γ	0.10 μM
k_{flux}	16.0 $\mu\mathrm{M} \cdot \mathrm{s}^{-1}$
μ_0	0.29
μ_1	0.30
k_μ	4.0 μM
D_c	20 $\mu\mathrm{m}^2 \cdot \mathrm{s}^{-1}$
D_p	300 $\mu\mathrm{m}^2 \cdot \mathrm{s}^{-1}$

Figure 1: Mckenzie and Sneyd

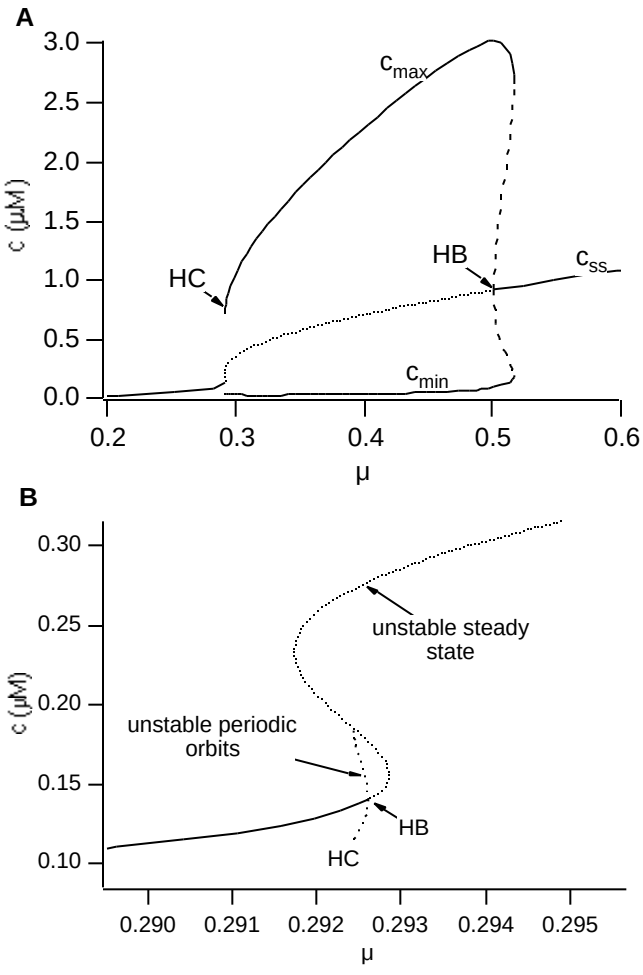

Figure 2: Mckenzie and Sneyd

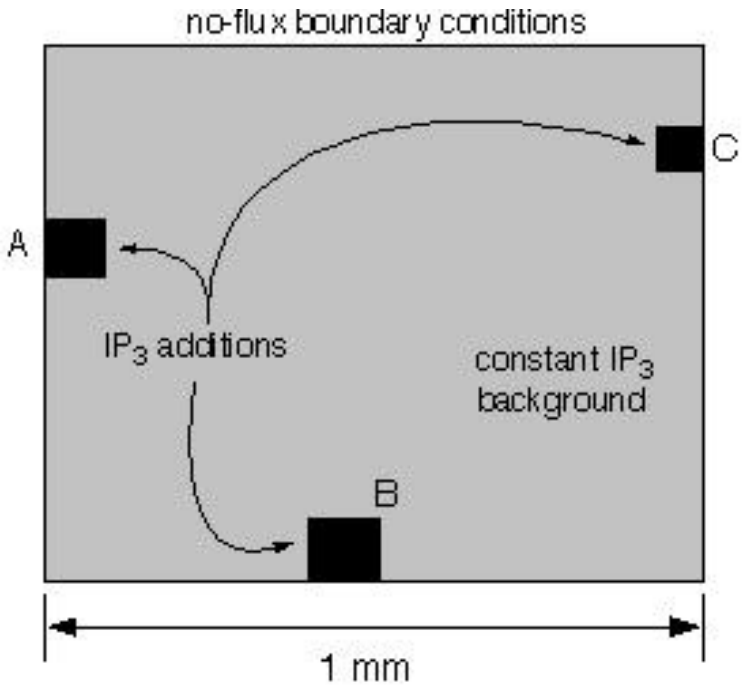

Figure 3: Mckenzie and Sneyd

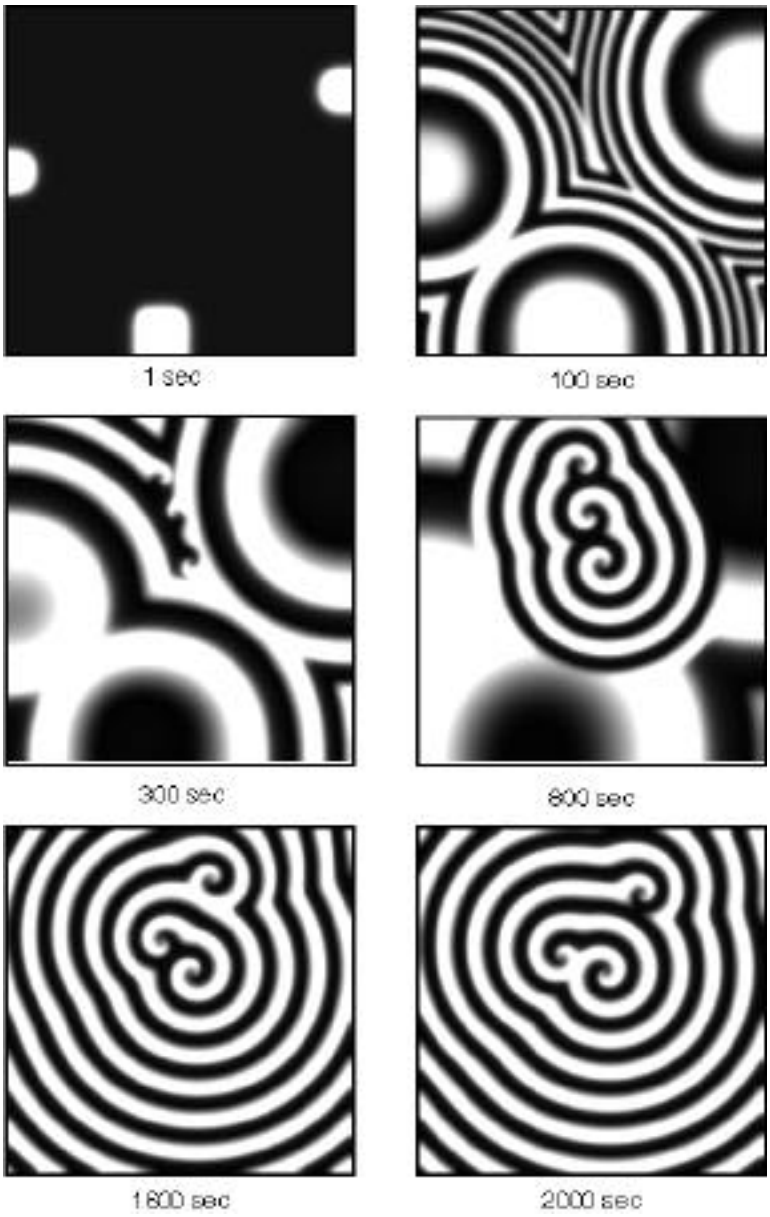

Figure 4: Mckenzie and Sneyd

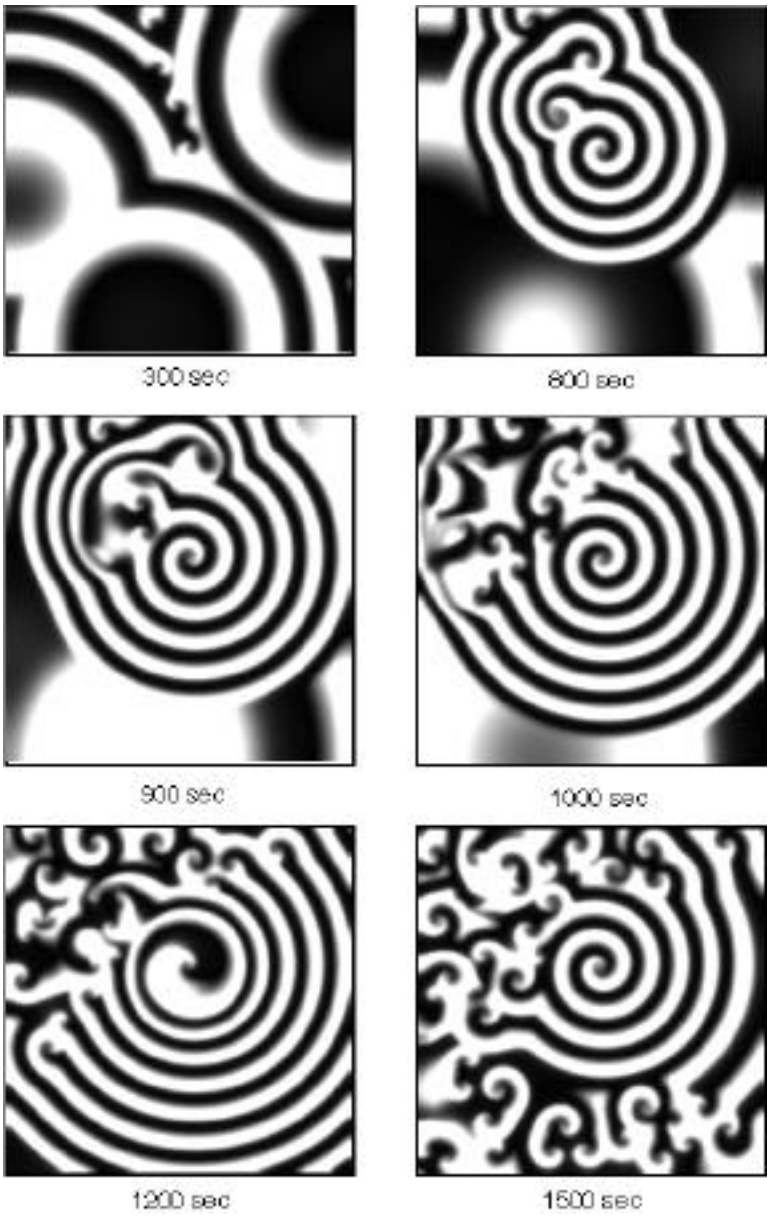

Figure 5: Mckenzie and Sneyd

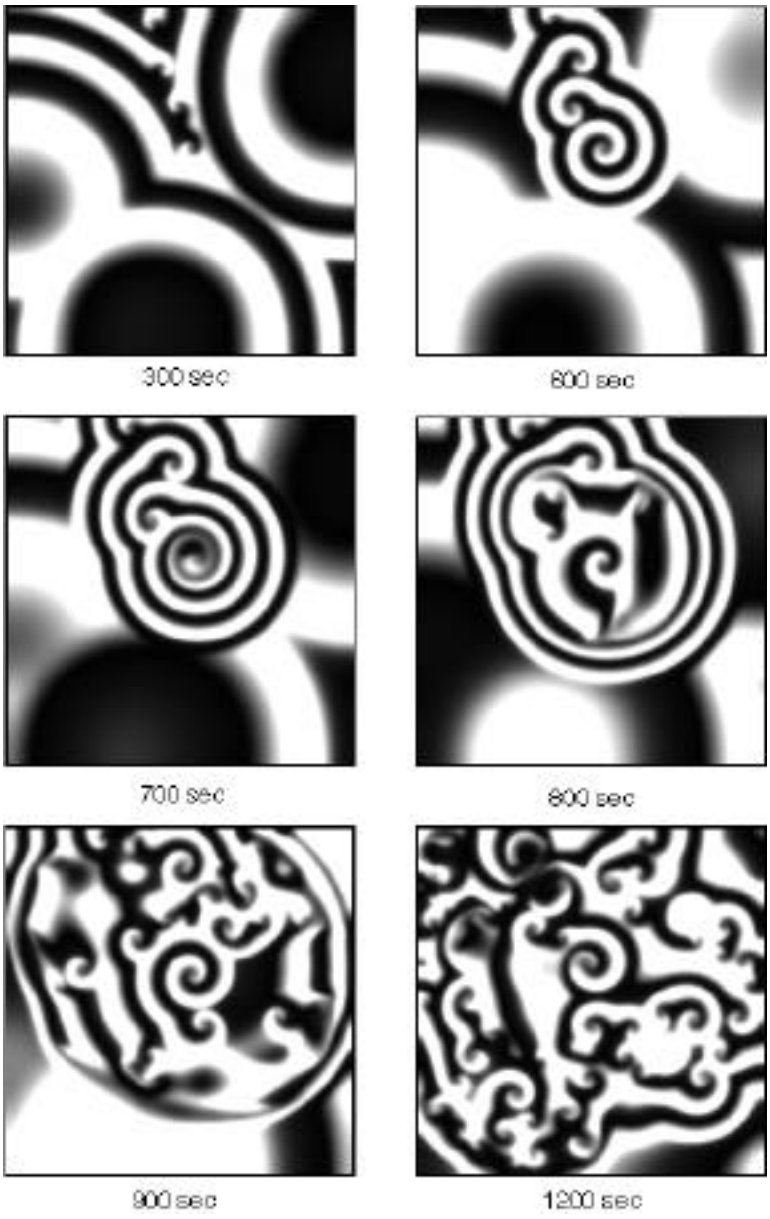

Figure 6: Mckenzie and Sneyd

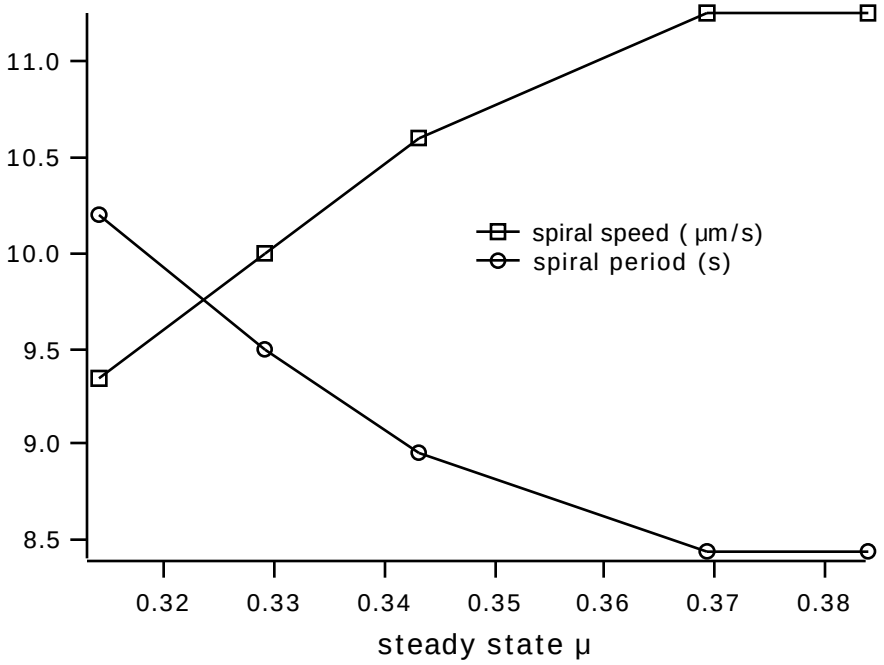

Figure 7: Mckenzie and Sneyd